# IMPLEMENTATION OF A PHOTOGRAMMETRIC RANGE SYSTEM

**Antonio Maria Garcia Tommaselli**
*Head of the Department of Cartography*
**Milton Hirokazu Shimabukuro**
*Software Engineer*
**Patrícia A. Paiola Scalco**
**Fernando M. A. Nogueira**
*Undergraduate Students*

**São Paulo State University - Unesp**
*Campus Presidente Prudente, S.P.*
*e_mail: ueppr@eu.ansp.br*
**BRAZIL**

Commission III, Working Group 2

**KEY WORDS:** Reconstruction, Triangulation, Metrology, Vision, Automation, Close_Range Digital Scanner, Three-dimensional Reconstruction.

## ABSTRACT

This paper describes the implementation of a Photogrammetric Close Range system which aims near real time object reconstruction. The system is based on off-the-shelf video and a pattern projector. Stereo configuration is avoided due to the high computational costs of the matching procedure. The mathematical model of the object reconstruction and calibration is based on the parametric equation of the projected straight line combined with collinearity equations. The derivation of the mathematical model, methods for feature extraction and results obtained from simulated and real data are presented. A sequential approach to calibrate the projected bundle is discussed. Accuracy of 1/4 of the pixel size can be obtained with the $\theta$-$\rho$ grouping method and least squares line fitting. Experiments with simulated data have indicated 1mm of accuracy in height determination and 0.3mm in the XY plane in an application where the separation between object and camera was 1000mm.

## 1. INTRODUCTION

This paper is concerned with the current stage of a Photogrammetric Range System which has been developed at Unesp-Presidente Prudente, Brazil. A financial support of **CNPq** (National Research Council) has been available. The motivation of the project are the needs in surface measurements for applications in industry and medicine. Previous research projects were conducted using non-metric cameras to measure body surface shapes aiming clinical applications such as diagnosis of postural problems associated with scoliosis, mastectomy and other diseases. However, conventional analogue or analytical Photogrammetry cannot be applied to solve properly these new tasks because near real time responses and full automation are required, as well as low cost systems.

Automation is of crucial importance because non specialists in photogrammetry have to deal with the system routinely. The surface measurements must be accurate in order to derive high quality analysis of dimensions and/or deformations (Mitchell, 1995).

Digital Photogrammetry seems to fulfill these needs and high precise close range surface measurements can be achieved. The traditional stereo configuration is unsuitable to this specific task due to the computational costs of the stereo-matching procedure. An active pattern projector can be introduced and treated as an active camera and only one digital imaging camera is used. This is similar to triangulation with structured light (Guisser et al, 1992).

This paper presents the proposal and preliminary results of a photogrammetric system composed of low cost hardware, based on a pattern projector, an electronic camera and image processing software.

## 2. FEATURE EXTRACTION

### 2.1 Methods

The pattern projected onto the surface must be designed to make feasible image analysis in real time, for example, a set of cross lines, squares or dots. In order to improve the correspondence process it is recommended

to design a pattern with distinct spots, both in shape and dimension. A set of cross lines with varying orientation and number of lines and squares have been used in the implemented system.

Edge detection and vectorization are performed after image grabbing only at defined windows in the image. The feature extraction step attempts to detect, recognise and "measure" the projected lines onto the object. Edge detection is accomplished with Sobel operators calculating the magnitude and gradient orientation. Orientation histograms are computed from gradient orientation data for small sliding windows. The histogram analysis defines the number and orientation of edges in the window aiming target recognition and labelling. Edge pixels are then classified using three grouping steps: $\theta$-, $\rho$-, and xy-grouping. After edge grouping a least squares line fitting is performed (Tommaselli and Tozzi, 1996). The intersection of the adjusted straight lines defines the cross line center or the center of the square.

Least squares matching was also implemented to enable an alternative method for point detection, mainly detection of the central and peripheral squares.

The process of feature extraction is applied to small search windows. The first window to be scanned is a large area around the center of the image. In this search window a square must be detected. Once the central square is detected, peripheral squares surrounding the object must be detected. With these set of points located in the image, smaller search windows can be computed for the star shaped points. The last step is the search for the crosses within each small area defined by previously located points. Squares and cross lines can be recognised either by template matching or analysing the number and orientation of connected straight lines in the orientation histogram.

### 2.2 Accuracy of Feature Extraction

Experiments using real images, which were collected with the projected pattern over flat surfaces and other scenes were conducted. The least squares matching works properly with flat surfaces attending sub-pixel accuracy requirements.

However, the projected features are deformed in real surfaces and objects (a leg, or a torso, for example) and the least squares matching may fail. Even deformed geometric shapes (crosses) are still intersections of lines. As such, the adjusted straight line equations provided good results in these cases.

The experiments have shown an accuracy of 1/4 of the pixel size with the $\theta$-$\rho$ grouping method. Similar results were obtained with the least squares matching, but only with flat surfaces.

The results described above can be drastically improved. Trinder et al (1995) reported simulated experiments with precision of the order of 0.01 pixel.

## 3. PHOTOGRAMMETRIC INTERSECTION

The concept of our approach is to avoid inner calibration of the projector. Only each straight line equation of the projected bundle is computed instead of the inner orientation parameters of the projector (Tommaselli et al, 1995).

The mathematical model is based on the collinearity equations (eq. (1)), considering the global reference system coincident with the photogrammetric reference of the camera.

$$x_i = -f\frac{X_i}{Z_i} \qquad y_i = -f\frac{Y_i}{Z_i} \tag{1}$$

where **f** is the camera focal length;
$x_i$, $y_i$ are the image coordinates;
$X_i$, $Y_i$, $Z_i$ are the point coordinates in the object space;

The parametric equations of a projected straight line are given by:

$$X_i = X_o + \lambda_i l_i \qquad Y_i = Y_o + \lambda_i m_i \qquad Z_i = Z_o + \lambda_i n_i \tag{2}$$

where: $X_o$, $Y_o$, $Z_o$ are the coordinates of the perspective center of the projector;
$l_i$, $m_i$, $n_i$ are the direction cosines of the projected straight line;
$\lambda_i$ is a parameter;

Equations (2) combined with (1) gives the basic equations of the mathematical model:

$$x_i = -f\frac{X_o+\lambda_i l_i}{Z_o+\lambda_i n_i} \qquad y_i = -f\frac{Y_o+\lambda_i m_i}{Z_o+\lambda_i n_i} \tag{3}$$

The inner orientation parameters of the camera and the elements of the projected straight line ($X_o$, $Y_o$, $Z_o$ $l_i$, $m_i$, $n_i$) were previously computed in the calibration step (section 4). The parameter $\lambda_i$ is unknown and must be computed for each straight line using the least squares method. For each projected straight line two observation equations are generated with only one unknown ($\lambda_i$) and a least squares solution can be computed recursively, using equations (4).

$$\delta\lambda^j = -N^{-1}U \qquad \lambda^{j+1} = \lambda^j + \delta\lambda^j \tag{4}$$

where:

$$N^{-1} = \frac{[Z_o + \lambda_i n_i]^4}{f^2[(Z_o l_i - X_o n_i)^2 + (Z_o m_i - Y_o n_i)^2]}$$

$$U = -f\frac{[L_1(Z_o l_i - X_o n_i) + L_2(Z_o m_i - Y_o n_i)]}{(Z_o + \lambda_i n_i)^2}$$

and $L_1 = F(\lambda_0) - x_i$

$L_2 = F(\lambda_0) - y_i$

$\lambda_0$ is an approximate value for the parameter $\lambda_i$;

The $X_i$, $Y_i$, $Z_i$ coordinates of point $P_i$ can be computed using equations (2) and the adjusted $\lambda_i$.

## 4. CALIBRATION OF THE PROJECTED BUNDLE

The system calibration involves the determination of the camera inner orientation parameters and the parametric equations of all projected straight lines. This concept is depicted in figure 1.

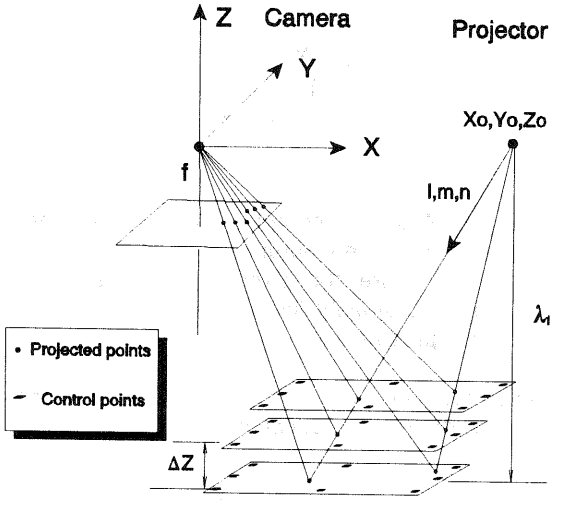


Fig. 1 Reference system and the geometric concept of the calibration method.

Although the simultaneous estimation of those parameters would be desirable, experiments demonstrated unreliable results and high computational costs. Considering this experience, a sequential solution was derived. It involves five steps, which are summarised in figure 2.

The concept of the calibration method is similar to the $\Delta Z$ method, used in triangulation by independent models. Several images of the projected bundle are acquired on the parallel reference planes which have targets to be

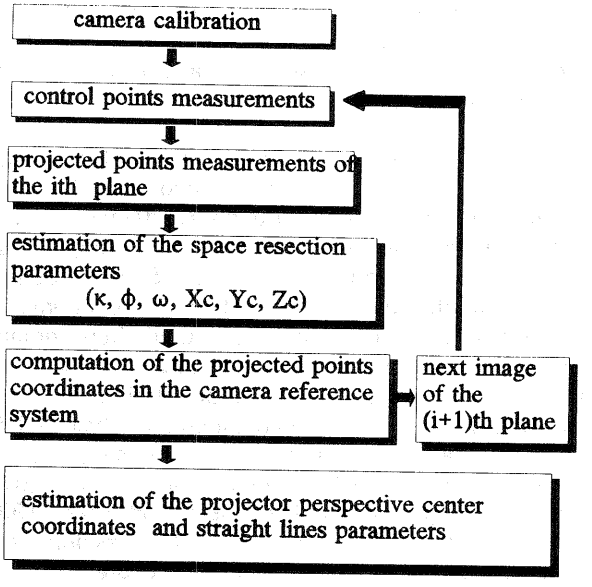


Fig. 2 Computation of the straight lines parameters

used as control points. Different image coordinates of one point in several planes will correspond to the same straight line in the object space. Control points are used to compute the plane position and orientation with respect to the camera reference system. Therefore, the coordinates of the projected points over the plane can be computed.

In the sequential approach the camera is firstly calibrated using self calibrating bundle adjustment with convergent cameras. The same structure of the range system can be used in this task. Previous experiments with real data have presented suitable results with four images and 20 control points.

The second step involves the features extraction of each image collected for the projection planes. The coordinates of the control and projected points are computed using the methods of feature extraction described in section 2.

Position and orientation parameters of the camera with respect to the control points are computed in the third step using Space Resection.

The fourth step attempts to compute the coordinates of the projected points in the camera reference system, using the position and orientation parameters previously computed.

Once the reference plane is moved, another image is grabbed and steps 2, 3 and 4 are repeated, until, at least, three planes are available.

Coordinates of the projector perspective center and straight lines parameters are estimated in the fifth step. These parameters are computed in a simultaneous least

squares adjustment. The observation equations are based on the parametric equations of the straight line (eq. (2)).

The vector of unknowns is:

$$Xa = [X_o, Y_o, Z_o, l_1, m_1, n_1, \ldots l_n, m_n, n_n, \lambda_1, \lambda_2, \ldots, \lambda_p]^T$$

where
$(l_n, m_n, n_n)$ are the direction cosines of the $n^{th}$ straight line;
$\lambda_p$ is the unknown distance between the perspective center of the projector and the $\mathbf{p^{th}}$ reference plane. The planes are supposed to be parallel to the camera reference system.

The vector of observations is:

$$Lb = [X^1_1, Y^1_1, Z^1_1, X^2_1, Y^2_1, Z^2_1, \ldots X^n_1, Y^n_1, Z^n_1, X^1_2, Y^1_2, Z^1_2, X^2_2, Y^2_2, Z^2_2, \ldots X^n_2, Y^n_2, Z^n_2, \ldots, X^1_p, Y^1_p, Z^1_p, X^2_p, Y^2_p, Z^2_p, \ldots X^n_p, Y^n_p, Z^n_p]^T$$

where the $X^n_p$, $Y^n_p$, $Z^n_p$ are the coordinates of the $n^{th}$ projected point over the $p^{th}$ reference plane. These coordinates were computed using the parameters of space resection for each plane.

A constraint must be introduced to eliminate correlation between $\lambda_1$ and the direction parameters $(l_i, m_i, n_i)$, otherwise the results will not converge. The simplest way to establish a constraint is to fix the $\lambda_1$ parameter. The direction vectors and the others $\lambda_i$ will be related to $\lambda_1$. Non normalised values of the direction vector parameters will be obtained. This means that:

$$l^2 + m^2 + n^2 \neq 1 \qquad (5)$$

After the simultaneous estimation process each direction vector can be individually normalised.

Another approach could be to establish the following constraint:

$$l^2 + m^2 + n^2 = 1 \qquad (6)$$

This option was also tested but the first one showed to be simpler and more efficient if the computational costs taken into account.

## 5. SURFACE FITTING AND INTERPOLATION

The obtained point coordinates in the object space define an irregular mesh of triangles. In order to generate a range image, a regular grid must be interpolated from the irregular data. Triangles could be selected using Delanay Triangulation but such approach is time consuming. In our approach, we have previously recognised each projected point. Using this knowledge it is more efficient to establish neighbourhoods and then apply an interpolation method considering a set of nine neighbour points. This interpolation scheme is based on the adjustment of a surface over the nine points which are represented by the following mathematical model:

$$Z = a + b.X + c.Y + d.X^2 + e.X.Y + f.Y^2 \qquad (7)$$

Selection of points to be used in the adjustment can be carried out using the minimum distance criteria. The central point of a 3x3 matrix is the closest with the points to be interpolated (points of the regular grid).

The interpolated regular grid can be transformed into a range image associating a pixel to the Z coordinate. This range image is suitable for automatic analysis in practical applications of measuring volumes, dimensions, shapes and deformations.

## 6. RESULTS

### 6.1 System Calibration

Results obtained with the proposed mathematical model of system calibration using simulated data are presented. Inner orientation parameters of the camera were supposed to be known from a previous camera calibration with self calibrating convergent cameras.

#### 6.1.1 Simulated Data

In order to verify the accuracy of the proposed sequential system calibration, simulated data were generated using the following camera parameters: 10mm focal length, 5x4 $mm^2$ imaging area, and 10x10 $\mu m^2$ pixel size. The position of the perspective center of the projector was supposed to be ($X_0 = 300$mm, $Y_0 = 10$mm, $Z_0 = 10$mm), with respect to the camera reference system.

Eight control points were introduced in the projection plane. Fifteen points were projected onto the projection plane which was moved at three different positions with respect to the camera:
-1050mm, -900mm, -750mm. It means that the separation ($\Delta Z$) between each projection plane was 150mm. The geometric configuration of the control and projected points and the projection planes are presented in the figure 3.

Object coordinates of the projected points onto the $\mathbf{p^{th}}$ reference plane were obtained from the parameters of the projected straight lines. These parameters were computed from the simulated image coordinates of a grid located in the projector.

Finally, image coordinates of projected and control points were computed using the collinearity equations. Random errors with a standard deviation of 3$\mu$m were introduced in the image. This error is equivalent to 1/3 of the pixel size and can be easily obtained by any of the presented feature extraction methods.

The simulated data consist of a set of image coordinates of control and projected points over three reference planes.

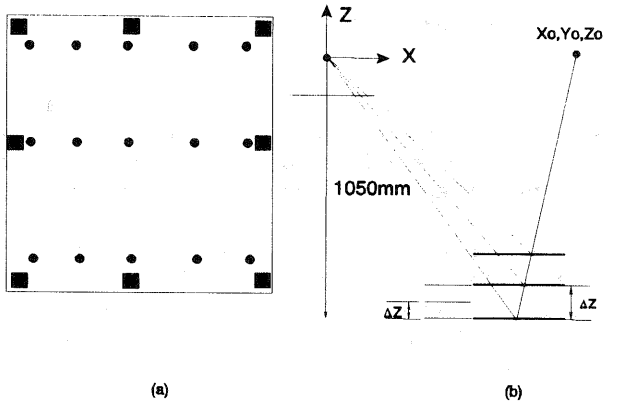


Fig. 3 Configuration of the simulated data
(a) projected and control points;
(b) separation between the reference planes;

As explained earlier a constraint must be introduced. In this case, the $\lambda_1$ (plane 1050mm apart from the camera) was fixed as:

$\lambda_1 = 1050$ mm

The same procedure was used to generate a second set of simulated data with a smaller ΔZ (50mm). The projection planes were supposed to be at:

$Z_1 = -1050$mm; $Z_2 = -1000$mm and $Z_3 = -950$mm

### 6.1.2 Calibration results

In order to analyse the experiments the estimated values ofthe parameters are compared with the true ones, which are known from the simulated data. The *true error* ($\epsilon_v$) can be defined as the difference between the estimated and the true parameter values. The standard deviation is defined as the square root of the estimated variance. As several groups of parameters were estimated (direction cosines for several projected lines) the mean-square values of the true errors ($\epsilon_{vm}$) were also computed encompassing all the projected points.

With the simulated data available, space resection parameters of the camera were obtained and used to compute object space coordinates of the projected points lying at the $\mathbf{p}^{th}$ reference plane. This process is repeated for all reference planes. The discrepancies between the true and the computed values, at the first plane (1050mm), for the XY and Z coordinates are within 0.3mm and 1mm respectively.

The coordinates of the projected points for the three reference planes were used as observations in order to estimate the coordinates of the projector perspective center and the direction vectors of the projected straight lines.

Table 1 Results of the two case studies with different separation for the reference planes

| | ΔZ = 100mm | | ΔZ = 50mm | |
|---|---|---|---|---|
| | $\epsilon_v$ | $\sigma_x$ | $\epsilon_v$ | $\sigma_x$ |
| $l_i$ | 0.0076 | 0.0005 | 0.0069 | 0.002 |
| $m_i$ | 0.0090 | 0.0005 | 0.0091 | 0.0018 |
| $n_i$ | 0.0372 | 0.0016 | 0.0362 | 0.0079 |
| $X_0$ | 0.383 | 0.420 | 0.492 | 2.069 |
| $Y_0$ | 0.251 | 0.370 | 1.079 | 1.825 |
| $Z_0$ | 0.293 | 1.691 | 1.498 | 8.333 |

Results obtained from the two sets of simulated data (ΔZ = 100mm and ΔZ = 50mm) are presented in table 1. The mean-square values of the true errors of the estimated direction parameters and the true error for the projection center are presented in the first and third columns. The estimated standard deviations are presented in the second and fourth columns. The estimated standard deviations are similar for all the projected straight lines. The coordinates are given in millimeters and the direction cosines are undimensional. No significant improvement in the accuracy of the direction cosines could be verified as an effect of a greater ΔZ. However, the coordinates of the projection center were better estimated with a larger ΔZ (100mm). The estimated standard deviations of the projection center and the direction cosines are higher in the second case (smaller ΔZ, 50mm). With these results we can conclude that a stronger geometry is obtained in the first case, in which a greater separation (ΔZ) between reference planes was used.

Table 2 Residuals of the XYZ coordinates after estimation of the projector parameters

| | ΔZ = 100mm | ΔZ = 50mm |
|---|---|---|
| | MSV | MSV |
| $r_X$ | 0.302 mm | 0.244 mm |
| $r_Y$ | 0.276 mm | 0.317 mm |
| $r_Z$ | 0.232 mm | 0.577 mm |

Table 2 presents the mean-square value of the residuals in the X, Y and Z coordinates after the estimation of the projector parameters, for both cases. It can be verified that these residuals were similar for both cases, except in the Z coordinates for the second case, which were higher. Notice that in all cases these residuals were smaller than 1mm.

Using the estimated projected parameters and the intersection procedure presented in section 3, the coordinates of the projected fifteen points were computed using the first reference plane and the

Table 3 Errors in the projected points over the reference plane.

| | ΔZ = 100 mm | | ΔZ = 50 mm | |
|---|---|---|---|---|
| | $\epsilon_{vm}$ | $\sigma_x$ | $\epsilon_{vm}$ | $\sigma_x$ |
| $X_i$ | 0.382 | 0.67 | 0.348 | 2.99 |
| $Y_i$ | 0.275 | 0.63 | 0.269 | 2.66 |
| $Z_i$ | 1.525 | 0.63 | 0.853 | 2.66 |

simulated image coordinates. The estimated coordinates using this intersection approach and the true coordinates, which were known from the simulation, were compared. The mean-square values for the true errors of the fifteen points coordinates are presented in the first and third columns of the table 3. The second and third columns show the estimated standard deviations for those coordinates. These deviations were obtained using covariance propagation from the equations (3) (Tommaselli et al, 1995). These results can be interpreted as the expected accuracy of the range system. The mean-square values of the true errors in the projected coordinates were similar in the two cases. However, in the second one the estimated standard deviations were higher, probably due to a worse configuration.

## 7. CONCLUSION

All computer software were written in C language, including the image processing routines. The obtained results with the proposed Photogrammetric Range System using simulated data seems to be suitable to the proposed applications. Variations in the calibration geometry give very accurate results. Feature extraction methods were tested and now improvements in the algorithms are being introducing in order to obtain higher accurate image coordinates.

The results obtained indicated that 1mm of accuracy in height determination and 0.5mm in XY plane can be reached, in a typical application. Some questions associated with feature extraction must be further studied aiming the improvement of the whole accuracy of the system.

## 7. REFERENCES


GUISSER, L.; PAYRISSAT, R.; CASTAN, S. A New 3-D Measurement System Using Structured Light, IEEE, 1992.

MITCHEL, H.L. Applications of digital photogrammetry to medical investigations. **ISPRS Journal of Photogrammetry & Remote Sensing,** Vol. 50, N. 3, 1995.

TOMMASELLI, A.M.G.; TOZZI, C.L. A recursive approach to Space Resection using straight lines. **Photogrammetric Engineering and Remote Sensing**. 1996.

TOMMASELLI, A.M.G.; SHIMABUKURO, M.H.; SCALCO, P.A.P.; NOGUEIRA, F.M.A. Photogrammetric Range System: Mathematical Model and Calibration. In: Proceedings of the Third Conference on Optical 3-D Measurement Techniques, Viena, 1995.

TRINDER, J.C.; JANSA,J.; HUANG, Y. An assessment of the precision and accuracy of methods of digital target location. **ISPRS Journal of Photogrammetry & Remote Sensing,** Vol. 50, N. 2, 1995.